Chinese Chemical Letters 35 (2024) 108225

Contents lists available at ScienceDirect

Chinese Chemical Letters

journal homepage: www.elsevier.com/locate/cclet

Carbon dots-incorporated $CuSeO_3$ rationally regulates activity and selectivity of the hydrogen species *via* light-converted electrons

Yuqi Ren[a], Hongxu Zhang[a], Caihong Hao[a], Qing Chang[a], Ning Li[a], Jinlong Yang[a,b], Shengliang Hu[a,*]

[a] *Research Group of New Energy Materials and Devices, North University of China, Taiyuan 030051, China*
[b] *State Key Laboratory of New Ceramics and Fine Processing, Tsinghua University, Beijing 100084, China*

ARTICLE INFO

Article history:
Received 11 December 2022
Revised 6 February 2023
Accepted 12 February 2023
Available online 16 February 2023

Keywords:
Heterostructure
Carbon dots
Photocatalysis
Chemoselective hydrogenation
Copper selenite

ABSTRACT

The chemoselective hydrogenation of structurally diverse nitroaromatics is a challenging process. Generally, catalyst activity tends to decrease when excellent selectivity is guaranteed. We here present a novel photocatalyst combining amino-functionalized carbon dots (N-CDs) with copper selenite nanoparticles (N-CDs@$CuSeO_3$) for simultaneously improving selectivity and activity. Under visible light irradiation, the prepared N-CDs@$CuSeO_3$ exhibits 100% catalytic selectivity for the formation of 4-aminostyrene at full conversion of 4-nitrostyrene in aqueous solvent within a few minutes. Such excellent photocatalytic performance is mainly attributed to the precise control of the hydrogen species released from the ammonia borane by means of light-converted electrons upon N-CDs@$CuSeO_3$. Besides, the defect states at the interface of N-CDs and $CuSeO_3$ enable holes to be trapped for promoting separation and transfer of photogenerated charges, allowing more hydrogen species to participate in catalytic reaction.

Functionalized anilines are critical to the manufacture of polymers, fertilizers, medicines, dyes, and other fine and bulk chemicals [1–5]. Normally, their production mainly relies on noncatalytic reduction of the corresponding nitroarenes taking advantage of stoichiometric reductants including sodium hydrosulfite, Fe, Sn, Zn in ammonium hydroxide [6–9]. Such processes, however, suffer from serious environmental issues, low selectivity and a great number of byproducts. Catalytic selective reduction with supported noble metal catalysts (Pt, Pd, Au, *etc.*) has been developed as an environmentally benign and highly efficient approach towards the synthesis of fine chemicals and fuels from renewable and sustainable feedstock [8,10–13]. Given their high cost and limited availability, more earth-abundant alternatives and low-cost heterostructures/nanocomposites are spurred for use in selective hydrogenation of organic compounds. Nevertheless, currently catalytic hydrogenation reaction usually requires a relatively high temperature, high hydrogen pressure and long reaction time to proceed. This still causes high cost and fossil energy consumption as well as eco-environmental problems [14–17].

Ammonia borane (AB) is regarded as a safe, mild and affordable reagent. At room temperature, AB releases hydrogen species onto the surface of the catalyst and then uses hydrogen species to reduce the nitroaromatic hydrocarbons to their amine derivatives for hydrogenation [18]. Unfortunately, AB also faces some serious issues, such as low efficiency, invalid release of hydrogen species and high alkaline environment during the hydrolysis process. Particularly, AB-induced hydrogenation process becomes more complicated and shows poor selectivity while another reducible functional group (*e.g.* C=C, C=O, C≡C and C≡N) is present in the structure of nitro-aromatics [19–21]. Therefore, it is highly desirable for a truly efficient method that enables the release of hydrogen species from AB over heterogeneous catalysts to precisely meet chemoselective hydrogenation reaction, avoiding unnecessary wastes of AB.

Carbon dots (CDs) as a promising nanocatalysis platform are attracting great attention because of their chemical stability, low cost, unique properties of photoinduced charge transfer and storage [22–26]. Due to a variety of functional groups such as -OH, -COOH and -NH_2 on their surfaces [27–31], CDs tend to coordinate with metal ions; thereby they serving as heterogeneous nucleating agents can induce nucleation and growth of metal and their-related compound nanocrystals during heat treatment as well, leading to new heterostructures/nanocomposites. When used as photocatalysts for performing various catalytic reactions, these CDs-contained nanocomposites often exhibit the enhanced visible light absorption and higher efficiency for charge separation and transfer compared to the single nanophase [32]. Accordingly, using

* Corresponding author.
E-mail address: hsliang@yeah.net (S. Hu).

https://doi.org/10.1016/j.cclet.2023.108225
1001-8417/

CDs as nucleating agents holds great potential for obtaining ideal bi- and multi-component photocatalysts for artificial photosynthesis and organic matter transformation [24,26,33,34]. Additionally, it has been demonstrated that the presence of an active lone-pair of electrons on the Se^{4+} centers can play a key role in the crystalline architecture of this family of compounds, determined by the requirement of empty space to accommodate the selenium lone-pair electrons [35]. Accordingly, the combination of the inherently asymmetry of $(SeO_3)^{2-}$ with various transition metals enables a rich structural chemistry in transition metal selenites. Cupric selenite ($CuSeO_3{\cdot}2H_2O$) exhibits a broad absorbance in visible spectrum range and superior catalytic performance owing to the presence of abundant oxygen/selenium vacancies [36].

In this contribution, we employed amino-functionalized CDs (N-CDs) as heterogeneous nucleating agents to modulate the nucleation and growth of $CuSeO_3$ during hydrothermal conditions, acquiring a new photocatalyst of N-CDs@$CuSeO_3$ for the first time. Not only does N-CDs@$CuSeO_3$ possess superior visible light harvesting and charge separation efficiency, but also show a unique ability to precisely control the hydrogen species released from the AB *via* photogenerated electrons. As a consequent, we achieved an almost 100% selectivity in aqueous solution for the formation of 4-aminostyrene (4-AS) at 100% conversion of 4-nitrostyrene (4-NS) within 12 min of light irradiation time at room temperature.

The sample of N-CDs@$CuSeO_3$ catalyst was prepared by co-precipitation at 130 °C with SeO_2 as the selenite precursors and $CuSO_4$ as the precipitation agent in the prescience of N-CDs.

For comparison, we also prepared the other sample using the same process except for no adding N-CDs and named as $CuSeO_3$. Fig. 1a shows the X-ray diffraction (XRD) patterns of as-prepared samples. Negligible changes are observed in both sample patterns and their peaks are well matched with the crystalline $CuSeO_3{\cdot}2H_2O$ (JCPDS 17-00523), indicating that the $CuSeO_3$ are successfully synthesized. Nevertheless, the diffraction peaks of N-CDs cannot be clearly observed, possibly because of relatively low crystallinity of the carbogenic cores of the N-CDs (Fig. S1 in Supporting information). To determine whether N-CDs are successfully incorporated into $CuSeO_3$, we thereby performed X-ray photoelectron spectrum (XPS) survey analysis. As shown in Fig. 1b, N-CDs@$CuSeO_3$ sample displays a new peak of N element and an obvious peak of C element, which should derive from N-CDs, compared with $CuSeO_3$. The Se $3d_{5/2}$ XPS reveals a few contents of Se^{2-} in the pure $CuSeO_3$, whereas this case is not present in N-CDs@$CuSeO_3$ (Fig. S2a in Supporting information). It should be attributed to the formation of copper selenides in the presence of *N*-dimethylformamide (DMF), which can act as a reducing agent in hydrothermal conditions [37]. This deduction is also supported by Cu $2p_{3/2}$ XPS spectra (Fig. S2b in Supporting information). Adding N-CDs could facilitate the nucleation of $CuSeO_3$ through the coordination interaction of Cu^{2+} ions with amine groups on the surface of CDs, thereby inhibiting the reduction reaction between DMF and $SeO_3{}^{2-}$. Furthermore, the C–O, C=O, C–N, N–O and Cu-N are also observed in C 1s and N 1s XPS spectra, indicating the presence of N-CDs in N-CDs@$CuSeO_3$, (Figs. S2c and d in Supporting information). The ultraviolet–visible light (UV–vis) diffuse reflection spectroscopy was used to study the light absorption properties of as-prepared samples. From Fig. 1c, the sample of $CuSeO_3$ possesses good absorption from UV to the whole visible light spectrum, while the combination of N-CDs with $CuSeO_3$ enables the visible light absorption to enhance significantly in intensity.

The transmission electron microscopy (TEM) image shows the $CuSeO_3$ sample is a micron-sized aggregation composed of numerous spherical nanoparticles (Fig. S3a in Supporting information). The corresponding high resolution TEM (HRTEM) image reveals the clear lattice fringes with the distance of 0.5 nm, corresponding to the $CuSeO_3$ (110) crystalline plane (Fig. S3b in Supporting information). In contrast, a typical flake morphology feature is present in TEM images of N-CDs@$CuSeO_3$ (Fig. S3c in Supporting information). Further HRTEM image indicates that the presented flake consists of a great number of ultrafine nanocrystals with distinct heterogeneous interfaces (Fig. S3d in Supporting information), verifying that N-CDs serving as heterogeneous nucleating agents promote the nucleation and growth of $CuSeO_3$. Specifically, the fringes with the interplanar spacing of 0.32 and 0.5 nm presented in nanocrystals are assigned to the (002) crystal plane of N-CDs and (110) crystal plane of $CuSeO_3$, respectively. Elemental mapping images in Fig. S3e (Supporting information) reveal that Cu, Se, C and N elements are uniformly dispersed within the N-CDs@$CuSeO_3$ matrix, confirming the combination of N-CDs with $CuSeO_3$. According to above results, N-CDs as nucleation agents could promote the nucleation of $CuSeO_3$ and suppress their growth process, resulting in new morphologies and structures.

In order to verify the activity and selectivity of $CuSeO_3$ and N-CDs@$CuSeO_3$, selective hydrogenation of 4-NS was carried out in aqueous solution without adding any sacrificial reagent at room temperature (25 °C), using AB as reducing agent. Compared to organic solvents, water is able to permit AB to release hydrogen species faster [37], realizing highly efficient utilization of AB. Generally, the catalytic hydrogenation of 4-NS can transform into three distinct products (Fig. 2a): 4-AS, 4-nitroethylbenzene (4-NE), and 4-ethylaniline (4-EA). From Fig. 2b, 4-NS as well as three products 4-AS, 4-NE and 4-EA have distinct characteristic absorption peaks at 311, 273, 280 and 234 nm, respectively. As thus, optical absorption spectroscopy can be used to monitor catalytic transformation processes of 4-NS in real time.

When $CuSeO_3$ as a catalyst was added to 4-NS and AB solutions without illumination, the peak at 311 nm gradually decreased while a new peak appeared at 273 nm ascribing to the formation of 4-AS product (Fig. 2c). The catalytic reaction was stopped in 48 min. In contrast, the catalytic reaction was terminated in 18 min under visible light irradiation and the absorbance of the characteristic peak at 273 nm increased significantly (Fig. 2d), indicating more 4-AS production. Then, the catalytic performances of N-CDs@$CuSeO_3$ were examined under the same conductions. From

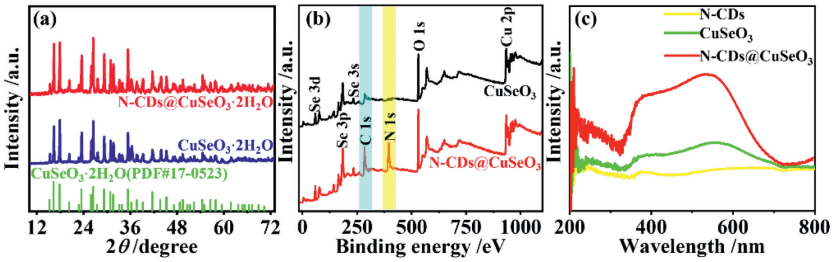

Fig. 1. (a) XRD patterns of as-prepared samples of $CuSeO_3$ and N-CDs@$CuSeO_3$; (b) XPS survey spectra of $CuSeO_3$ and N-CDs@$CuSeO_3$ samples; (c) UV–vis absorption spectra of N-CDs, $CuSeO_3$ and N-CDs@$CuSeO_3$.

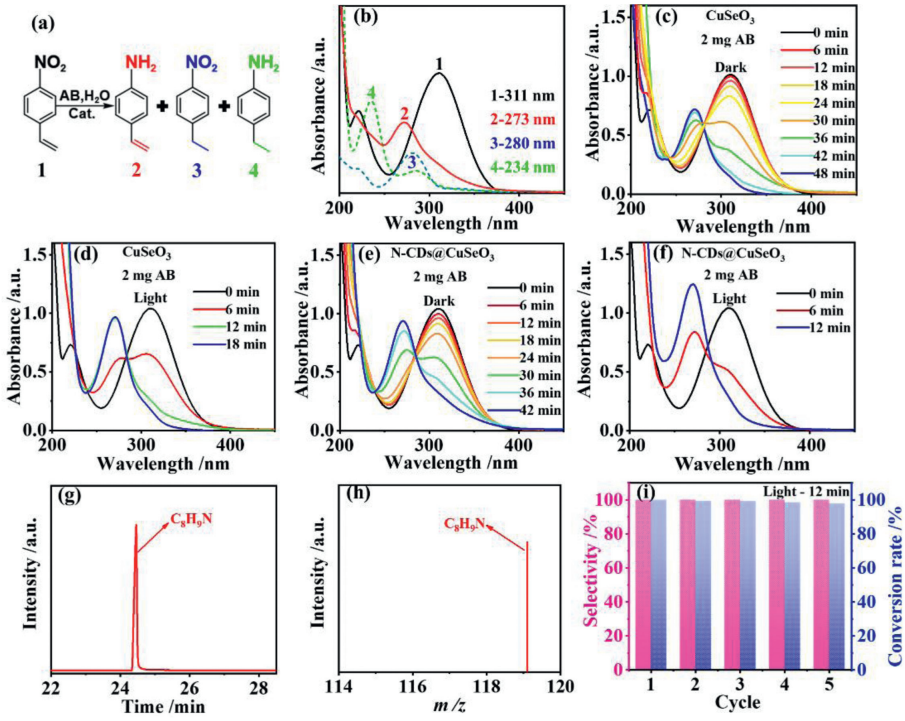

Fig. 2. (a) Diagram of raw material and three products; (b) The aqueous solution of pure 4-NS (1), 4-AS (2), 4-NE (3) and 4-EA (4) of UV–vis absorption spectra; (c, d) The evolution of 4-NS solution with time in the presence of $CuSeO_3$ without illumination (c) and with illumination (d); (e, f) The evolution of 4-NS solution with time in the presence of N-CDs@$CuSeO_3$ without illumination (e) and with illumination (f); (g) GC spectra of the product after catalytic reaction for 12 min over N-CDs@$CuSeO_3$; (h) MS spectra of the product after catalytic reaction for 12 min over N-CDs@$CuSeO_3$; (i) The cycling stability of N-CDs@$CuSeO_3$.

Fig. 2e, N-CDs@$CuSeO_3$ exhibited better selective reduction of -NO_2 than $CuSeO_3$ under dark condition. On illumination, the conversion of 4-NS into 4-AS was 100% in 12 min (Fig. 2f). Moreover, we further confirmed the reactants and products by gas chromatography-mass spectrometry (GC-MS) after 12 min reaction. The results revealed that all the 4-NS was completely converted to the target product 4-AS (Figs. 2g and h). For easy comparison, the activity and selectivity of both samples with and without illumination were summarized in Table S1 (Supporting information). It is clearly demonstrated that both samples possess excellent selectivity, but the introduction of N-CDs into $CuSeO_3$ can significantly enhance the activity. After 5 cycles of stability tests, more importantly, N-CDs@$CuSeO_3$ maintained its initial selectivity with only a negligible decrease in activity (Fig. 2i). Meanwhile, by XRD characterization for the recycled samples, the crystalline structure of N-CDs@$CuSeO_3$ was unchanged (Fig. S4 in Supporting information), suggesting excellent stability. Compared to the reported various catalysts (Table S2 in Supporting information), clearly our N-CDs@$CuSeO_3$ performs in a superior manner.

In order to determine the roles of N-CDs in the photocatalytic performance, we first investigated the effects of the added amount of N-CDs on the catalytic activity of N-CDs@$CuSeO_3$. As shown in Fig. S5 (Supporting information), the conversion rate of 4-NS into 4-AS firstly enhances and then decreases with the increasing of the amount of N-CDs. The optimum value is around 10 mg for sample synthesis. For comparison, N-CDs were replaced by CDs without surface modification of $NH_3{\cdot}H_2O$ during synthetic processes, obtaining a new sample of CDs@$CuSeO_3$. The introduction of CDs into $CuSeO_3$ did not realize synergistic effect in the selective hydrogenation of 4-NS to 4-AS (Fig. S6 in Supporting information), implying the critical roles of amine groups in composite system. Moreover, we conducted the photocurrent response tests. From Fig. 3a, the photocurrent intensity of the N-CDs@$CuSeO_3$ is significantly higher than that of $CuSeO_3$ and N-CDs, suggesting that N-CDs can facilitate the separation of photogenerated charge through forming heterogeneous interfaces with $CuSeO_3$. It can be also confirmed by electrochemical impedance spectroscopy (EIS) spectra, in which the carrier transfer efficiency is distinguished with the radius of the semicircle in a Nyquist plot at high frequency [38–40]. As illustrated in Fig. 3b, the radius of the semicircle for N-CDs@$CuSeO_3$ is much smaller than that of $CuSeO_3$ and N-CDs. Accordingly, N-CDs@$CuSeO_3$ is endowed with a lower charge transfer resistance than $CuSeO_3$ and N-CDs, facilitating carrier transfer across the solid-liquid interface.

In addition, the energy level positions of N-CDs, $CuSeO_3$ and N-CDs@$CuSeO_3$ were determined by the band gaps calculated by absorption spectra and XPS valence spectra. Based on absorption spectra of N-CDs, $CuSeO_3$ and N-CDs@$CuSeO_3$, their optical band gaps were estimated to be 2.17, 1.90 and 2.15 eV using the Kubelka-Munk function, respectively (Figs. S7a–c in Supporting information). Then from XPS valence spectra (Figs. S7d–f in Supporting information), their valence band (VB) positions were determined as 2.72, 1.68 and 1.86 V *vs.* normal hydrogen electrode (NHE), respectively. Thus, their corresponding conduction band (CB) positions were also acquired as shown in Fig. S8 (Supporting information). It can be found that the VB and CB positions of $CuSeO_3$ are modulated slightly by N-CDs owing to the formation of new interface states between N-CDs and $CuSeO_3$. Fig. 3c illustrates the role of the interface defect levels in the charge separation and transfer [41–43]. On the one side, the photoinduced electrons in the CB of N-CDs readily transport to recombine with the holes generated in the VB of $CuSeO_3$ at the interface defect levels, which is similar to an all-solid-state Z-scheme photocatalytic system [44–46]. On the other side, N-CDs act as sacrifice agents of holes [18], inhibiting the migration of photogenerated holes from the bulk to the surface. Consequently, more photogenerated electrons from $CuSeO_3$ are able to participate in selectively catalytic hydrogenation reaction. To prove this proposition, the control experiments were con-

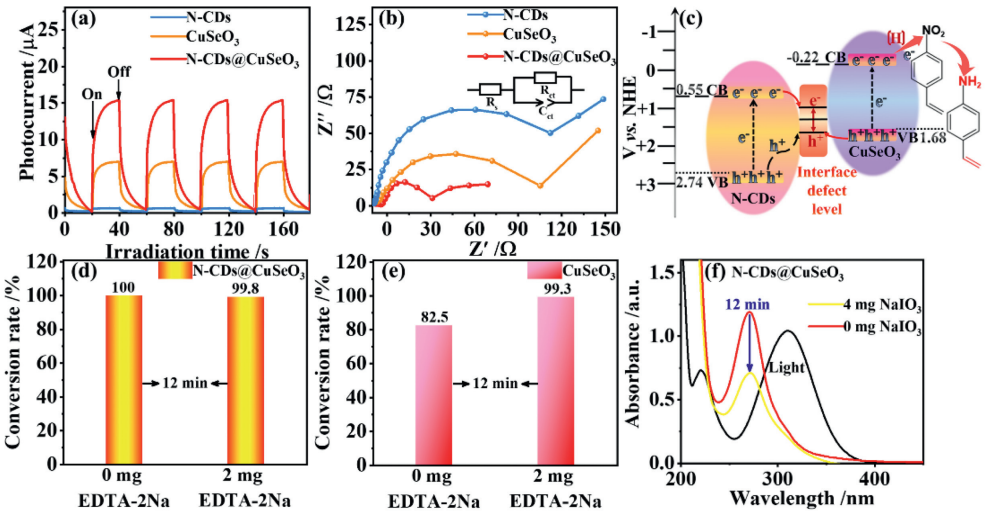

Fig. 3. (a) Photocurrent responses of N-CDs, $CuSeO_3$, N-CDs@$CuSeO_3$; (b) EIS plots of N-CDs, $CuSeO_3$, N-CDs@$CuSeO_3$; (c) Schematic illustration of the charge transfer processes in N-CDs@$CuSeO_3$ for chemoselective hydrogenation of 4-NS to 4-AS, in which h^+ and [H] represent the photogenerated hole and AB-released hydrogen species, respectively; (d) Comparison of the reaction activity of N-CDs@$CuSeO_3$ before and after adding EDTA-2Na while irradiating for 12 min; (e) Comparison of the reaction activity of $CuSeO_3$ before and after adding EDTA-2Na while irradiating for 12 min; (f) Comparison of the reaction activity of N-CDs@$CuSeO_3$ before and after adding $NaIO_3$ while irradiating for 12 min.

ducted with EDTA-2Na as the hole sacrificial agent. The addition of EDTA-2Na significantly increased the activity of $CuSeO_3$ to transform 4-NS to 4-AS, under visible light irradiation, whereas it did not influence the catalytic activity of N-CDs@$CuSeO_3$ (Figs. 3d and e). As expected, the catalytic activity of N-CDs@$CuSeO_3$ remarkably decreased when electron-sacrificing $NaIO_3$ was added in reaction system (Fig. 3f). All of above results indicate that only photogenerated electrons from $CuSeO_3$ can facilitate chemoselective reduction of 4-NS to 4-AS by AB.

Generally, the number of photogenerated electrons from photocatalysts depends on light intensity without changing other conditions. Since photogenerated electrons from $CuSeO_3$ can promote chemoselective reduction of 4-NS, their number increase could improve conversion rate of 4-NS to 4-AS in theory. However, we surprisingly found that the generation rate of 4-AS starts to decline after 6 min of reaction time with the increase of light intensity in the presence of N-CDs@$CuSeO_3$ catalyst (Fig. 4a). More interestingly, the amount of hydrogen evolution exhibits a similar rule with the generation rate of 4-AS relative to light intensities as well (Fig. 4b). This verifies that the activity of N-CDs@$CuSeO_3$ changes with irradiation time under higher light intensities. To explore the reason, we checked the pH values in the reaction system with reaction time under the different light intensities. From Fig. 4c, the pH values in the reaction system gradually increase with reaction time and light intensities, implying that the amount of AB hydrolysis upon N-CDs@$CuSeO_3$ highly relies on photogenerated electrons at the given time. The excessive decomposition of AB gives rise to an alkaline environment surrounding N-CDs@$CuSeO_3$ and so many NH_4^+ ions released that cannot diffuse from catalyst surface in time. Thereby, copper ammonia complexes ($[Cu(NH_3)_4]^{2+}$) could be formed by the reaction of NH_4^+ with $CuSeO_3$ in the proper pH conditions. The copper ammonia complexes covered at the surface prevent the adsorption of the catalyst on the hydrogen species released from AB, thus influencing the activity of catalysts.

Furthermore, we examined the catalytic activity of N-CDs@$CuSeO_3$ in different contents of AB at the given light intensity. When the added amount of AB is less than 2 mg under 10 mg of catalysts, chemoselective reduction of 4-NS to 4-AS cannot occur (Fig. S9 in Supporting information). As shown in Fig. 4d and Fig. S10 (Supporting information), overmuch AB in reaction system can also make the conversion rate of 4-NS to 4-AS decline significantly under visible light irradiation. Similarly, hydrogen evolution is also associated with the amount of AB (Fig. 4e). It is clear that more AB can create a higher pH environment surrounding N-CDs@$CuSeO_3$ and more NH_4^+ ions simultaneously, thus easily inducing the reaction of NH_4^+ with $CuSeO_3$ and causing the formation of copper ammonia complexes. What is noteworthy is that adding more AB in reaction system inversely boosts the conversion of 4-NS to 4-AS without illumination. Fig. 4f provides the pH variation with AB contents in the reaction system with and without illumination, respectively. It can be found that light irradiation considerably improves the pH values of reaction system. Therefore, light irradiation plays an important role in AB decomposition using N-CDs@$CuSeO_3$ as catalysts. Although the amount of catalysts can also affect the conversion rate of 4-NS to 4-AS, their activity does not decline with their increase because of no $[Cu(NH_3)_4]^{2+}$ production (Fig. S11 in Supporting information).

On the basis of above results, the photocatalytic mechanism of N-CDs@$CuSeO_3$ for selective hydrogenation of 4-NS is illustrated in Fig. 4g. When the number of photogenerated electrons matches with the requirements of hydrogenation reaction of 4-NS under the proper light intensity and AB content, all photogenerated electrons are allowed to involve in the catalytic reaction and efficiently improve the conversion rate of 4-NS to 4-AS (Case 1). When there are superfluous photogenerated electrons, the invalid AB decomposition could happen on the catalyst surface analogous to adding more AB. Just like Case 2 illustrated in Fig. 4g, excessive NH_4^+ ions that cannot diffuse in time will attack the $CuSeO_3$ in the suitable alkaline environment (*e.g.* pH > 8.05) and result in the formation $[Cu(NH_3)_4]^{2+}$ at the surface of catalysts. This can block the contact of 4-NS and/or AB with catalysts, weakening their activity. Accordingly, the utilized efficiency of AB-released hydrogen species in chemoselective reduction of 4-NS is determined by the number of inputted photons for our presented N-CDs@$CuSeO_3$.

In conclusion, we have developed a novel photocatalyst N-CDs@$CuSeO_3$ that can effectively utilize visible light in selective hydrogenation reaction at room temperature without adding any sacrificing reagents. Under visible light irradiation, our presented N-CDs@$CuSeO_3$ achieves 100% catalytic selectivity for the formation of 4-AS at full conversion of 4-NS in aqueous solvent within a few minutes. Meanwhile, N-CDs@$CuSeO_3$ possesses superior stability and can be used repeatedly. Such excellent catalytic perfor-

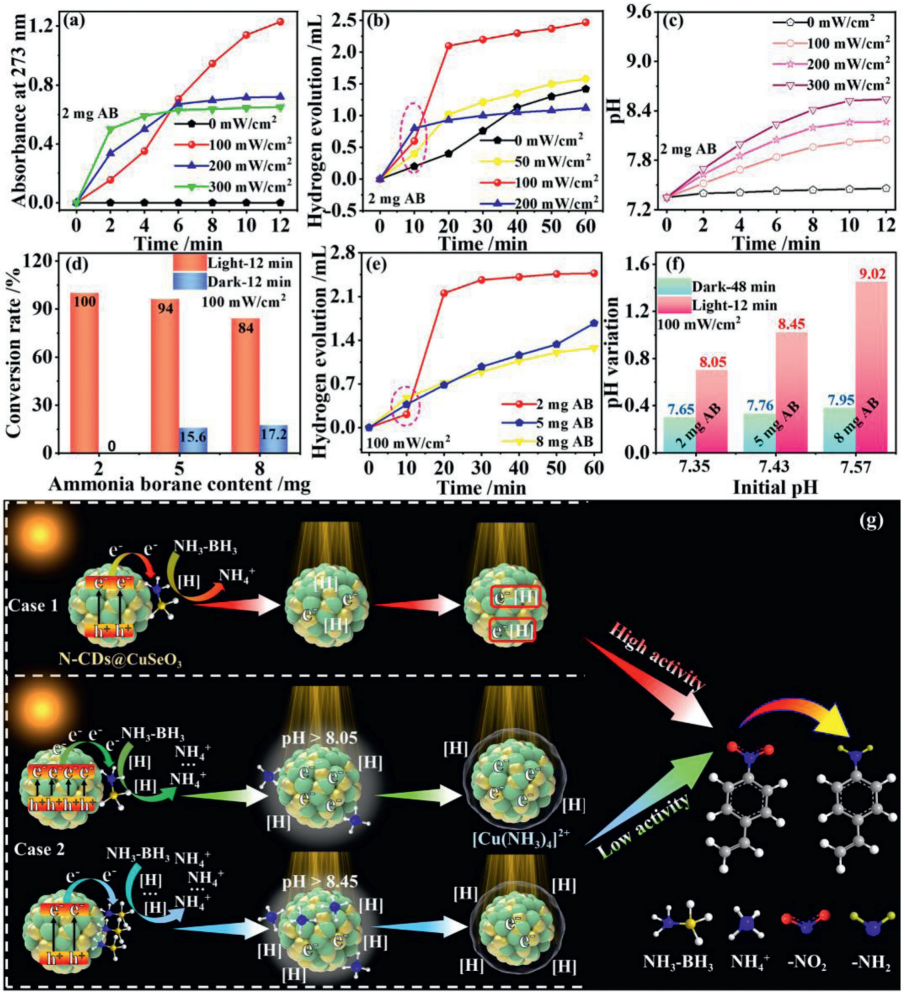

Fig. 4. (a) The evolution of 4-AS production rate with time in the presence of N-CDs@$CuSeO_3$ under different light intensities; (b) Hydrogen evolution amount with time in the presence of N-CDs@$CuSeO_3$ under different light intensities; (c) pH variations with irradiation time under different light intensities; (d) The dependence of conversion rate of 4-NS to 4-AS over N-CDs@$CuSeO_3$ on AB contents in reaction system without and with illumination; (e) Hydrogen evolution relative to AB contents in the presence of N-CDs@$CuSeO_3$; (f) pH changes in reaction system containing different AB contents under dark (48 min) and illumination (12 min); (g) Schematic illustration of the catalytic mechanism of N-CDs@$CuSeO_3$ for chemoselective hydrogenation of 4-NS upon irradiation.

mance has been demonstrated to stem from the precise control of the hydrogen species released from AB using light-converted electrons upon N-CDs@$CuSeO_3$. Besides, the defect states at the interface of N-CDs and $CuSeO_3$ enable holes to be trapped for promoting separation and transfer of photogenerated charges, allowing more hydrogen species to participate in catalytic reaction. Accordingly, this work demonstrates that CDs can be reasonably used to design ideal photocatalytic heterostructures for highly efficient organic conversion and synthesis using solar energy.

Declaration of competing interest

The authors declare that they have no known competing financial interests or personal relationships that could have appeared to influence the work reported in this paper.

Acknowledgments

We thank for financial support Fundamental Research Program of Shanxi Province of China (No. 20210302123037), Research Project Supported by Shanxi Scholarship Council of China (No. 2022-136) and Specialized Research Fund for Sanjin Scholars Program of Shanxi Province of China.

Supplementary materials

Supplementary material associated with this article can be found, in the online version, at doi:10.1016/j.cclet.2023.108225.

References

[1] M. Macino, A.J. Barnes, S.M. Althahban, et al., Nat. Catal. 2 (2019) 873–881.
[2] A.C.A.P. Serna, Science 313 (2006) 332–334.
[3] L. Wang, E. Guan, J. Zhang, et al., Nat. Commun. 9 (2018) 1362.
[4] Q. Wang, Q. Feng, Y. Lei, et al., Nat. Commun. 13 (2022) 3689.
[5] H. Wei, X. Liu, A. Wang, et al., Nat. Commun. 5 (2014) 5634.
[6] J. Mao, W. Chen, W. Sun, et al., Angew. Chem. Int. Ed. 56 (2017) 11971–11975.
[7] G. Sun, B. Xiao, H. Zheng, et al., J. Mater. Chem. A 9 (2021) 9735–9744.
[8] P. Verma, Y. Kuwahara, K. Mori, H. Yamashita, Catal. Today 324 (2019) 83–89.
[9] L. Zhang, J. Liang, L. Yue, et al., Nano Res. Energy 1 (2022) e9120028.
[10] A. Han, J. Zhang, W. Sun, et al., Nat. Commun. 10 (2019) 3787.
[11] Y. Lou, J. Xu, H. Wu, J. Liu, Chem. Comm. 54 (2018) 13248–13251.
[12] H. Song, J. Yu, Z. Tang, et al., Adv. Energy Mater. 12 (2022) 2102573.
[13] X. Sun, L. Sun, G. Li, et al., Angew. Chem. Int. Ed. 61 (2022) e202207677.
[14] J. CamachoBunquin, M. Ferrandon, H. Sohn, et al., J. Am. Chem. Soc. 140 (2018) 3940–3951.
[15] H. Ming, D. Wei, Y. Yang, et al., Chem. Eng. J. 424 (2021) 130296.
[16] C. Xia, S. Zhu, T. Feng, et al., Adv. Sci. 6 (2019) 1901316.
[17] X. Yang, X. Li, B. Wang, et al., Chin. Chem. Lett. 33 (2022) 613–625.
[18] Y. Ren, C. Hao, Q. Chang, et al., J. Mater. Chem. A 9 (2021) 25374–25380.
[19] H. Huang, C. Wang, Q. Li, et al., Adv. Funct. Mater. 31 (2020) 2007591.
[20] M. Shen, H. Liu, C. Yu, et al., J. Am. Chem. Soc. 140 (2018) 16460–16463.

[21] M. Tamura, N. Yuasa, Y. Nakagawa, K. Tomishige, Chem. Comm. 53 (2017) 3377–3380.
[22] K. Akbar, E. Moretti, A. Vomiero, Adv. Opt. Mater. 9 (2021) 2100532.
[23] X. Meng, C. Zhang, C. Dong, et al., Chem. Eng. J. 389 (2020) 124432.
[24] C. Rosso, G. Filippini, M. Prato, ACS Catal. 10 (2020) 8090–8105.
[25] H. Song, M. Wu, Z. Tang, et al., Angew. Chem. Int. Ed. 60 (2021) 7234–7244.
[26] L. Tian, Z. Li, P. Wang, et al., J. Energy Chem. 55 (2021) 279–294.
[27] Y. Chen, S. Ji, W. Sun, et al., Angew. Chem. Int. Ed. 59 (2020) 1295–1301.
[28] F. Li, N. Li, C. Xue, et al., Chem. Eng. J. 382 (2020) 122484.
[29] H. Nie, K. Wei, Y. Li, et al., Chin. Chem. Lett. 32 (2021) 2283–2286.
[30] X. Wang, M. Zhang, Y. Ma, et al., Appl. Surf. Sci. 583 (2022) 152540.
[31] P. Zhang, H. Liu, X. Li, A.C.S. Sustain, Chem. Eng. 8 (2020) 17979–17987.
[32] T.C. Wareing, P. Gentile, A.N. Phan, ACS Nano 15 (2021) 15471–15501.
[33] Y. Chen, J.F. L.i, P.Y. L.iao, et al., Chin. Chem. Lett. 31 (2020) 1516–1519.
[34] Y.Y. Liu, N.Y. Yu, W.D. Fang, et al., Nat. Commun. 12 (2021) 812.
[35] A. Larranaga, J.L. Mesa, L. Lezama, et al., Spectrochim. Acta A: Mol. Biomol. Spectrosc. 72 (2009) 356–360.
[36] L. Zhang, C. Lu, F. Ye, et al., Appl. Catal. B: Environ. 284 (2021) 119758.
[37] Y. Ren, C. Hao, Q. Chang, et al., Green Chem. 23 (2021) 2938–2943.
[38] M. Li, Z. Zhao, W. Zhang, et al., Adv. Mater. 33 (2021) 2103762.
[39] Y.Y. L.iu, H.L. Z.hu, Z.H. Z.hao, et al., ACS Catal. 12 (2022) 2749–2755.
[40] X. Zhang, F. Tian, X. Lan, et al., Chem. Eng. J. 429 (2022) 132588.
[41] S. Geng, F. Tian, M. Li, et al., Nano Res. 3 (2021) 1–8.
[42] F. Tian, S. Geng, L. He, et al., Chem. Eng. J. 417 (2021) 129232.
[43] X. Zhao, M. Huang, B. Deng, et al., Chem. Eng. J. 437 (2022) 135114.
[44] C. Liu, Y. Fu, J. Zhao, et al., Chem. Eng. J. 358 (2019) 142.
[45] Q. Xu, L. Zhang, J. Yu, et al., Mater. Today 21 (2018) 1042–1063.
[46] P. Zhou, J. Yu, M. Jaroniec, Adv. Mater. 26 (2014) 4920–4935.